

## An intentionally positioned (In,Ga)As quantum dot in a micron sized light emitting diode

M. Mehta,<sup>1</sup> D. Reuter,<sup>2</sup> A. D. Wieck,<sup>2</sup> S. Michaelis de Vasconcellos,<sup>1</sup> A. Zrenner,<sup>1</sup> and C. Meier<sup>1,a)</sup>

<sup>1</sup>Department of Physics and Center for Optoelectronics and Photonics Paderborn (CeOPP), University of Paderborn, Warburger Street 100, 33098 Paderborn, Germany

<sup>2</sup>Applied Solid State Physics, Ruhr-University of Bochum, Universitätsstr. 150, 44780 Bochum, Germany

(Received 1 July 2010; accepted 22 August 2010; published online 4 October 2010)

We have integrated individual (In,Ga)As quantum dots (QDs) using site-controlled molecular beam epitaxial growth into the intrinsic region of a p-i-n junction diode. This is achieved using an *in situ* combination of focused ion beam pre patterning, annealing, and overgrowth, resulting in arrays of individually electrically addressable (In,Ga)As QDs with full control on the lateral position. Using microelectroluminescence spectroscopy we demonstrate that these QDs have the same optical quality as optically pumped Stranski–Krastanov QDs with random nucleation located in proximity to a doped interface. The results suggest that this technique is scalable and highly interesting for different applications in quantum devices. © 2010 American Institute of Physics.  
[doi:10.1063/1.3488812]

Semiconductor quantum dots (QDs) (Ref. 1) are of great interest in the past and have great potential as building blocks for quantum information processing.<sup>2</sup> For such applications, lateral position control and electrical addressing are desirable. Most QD sources are pumped optically,<sup>2</sup> but many efforts toward electrical pumping have also been made.<sup>3–5</sup> At the same time, different approaches have been tried for site-selective growth of QDs.<sup>6–10</sup> In this work, we present an approach relying on focused ion beam (FIB) pre patterning of the sample with subsequent annealing. In the so formed nanodepressions, individual (In,Ga)As QDs nucleate that can be pumped electrically using a p-i-n junction diode. While other methods, such as growth of electron-beam-lithography<sup>8,9</sup> defined structures have some benefits, they still require *ex situ* preparation steps, such as etching for removal of material. In the reported work, we use an all-ultrahigh-vacuum (UHV) process to combine the molecular beam epitaxy (MBE) growth sequences with the FIB patterning steps. For removal of lattice damage, we employ an annealing and re-evaporation step, in which some part of the upper region of the sample is removed after the implantation step. This is a key prerequisite for the subsequent growth of the (In,Ga)As QDs.

Two different sample types have been studied. In the first series of experiments, samples without doped regions were grown in order to optimize the growth process and to study the QD structure and morphology. In the second series of experiments, using the optimized parameter set, site-controlled QDs were embedded in p-i-n junction devices and their electroluminescence (EL) was studied. The samples for the growth optimization consisted of the following layers: After a smoothing sequence, a 300 nm GaAs buffer layer was grown on GaAs (100) substrates at  $T=600$  °C using MBE. After these layers, the growth was interrupted and the sample was immediately transferred under UHV conditions to a FIB system ( $V_{\text{ACC}}=30$  kV,  $\text{Ga}^+$  ions). Here, the details of FIB patterning process can be found elsewhere<sup>10</sup>. Thereafter, the samples were retransferred to the MBE system,

where an *in situ* annealing step under arsenic atmosphere was performed. The best results have been achieved for  $T=760$  °C for 10 s, at which a re-evaporation of 3–5 nm GaAs occurs. At this point, the growth was terminated for a first subset of samples, which was used to study the surface morphology on the FIB modified spots via atomic force microscopy (AFM) and scanning electron microscopy (SEM). The second subset of samples was used to study the occupancy of QDs per spot after deposition of a varied amount of InAs [1.4–2.1 monolayers (MLs)] at 525 °C growth temperature. Here, the substrate temperature was monitored using an optical pyrometer.

For EL studies, after the buffer layer growth, a 145 nm thick silicon doped n-GaAs layer ( $N_{\text{D}}=2.5 \times 10^{18}$  cm<sup>-3</sup>) followed by a 15 nm undoped GaAs layer was grown at 600 °C. Then, using the optimized growth process, site-selective InAs QDs at 525 °C were deposited on the FIB patterned surface at growth rate of 0.013 ML/s. Subsequently, the QD layer was overgrown by 8 nm undoped GaAs at 515 °C. The reason for the overlayer growth at lower temperature is to minimize the In–Ga intermixing at the interface without In desorption from the QD surface. The substrate temperature where significant In desorption starts was tested using reflection high energy electron diffraction and was found to be around 535 °C. Afterwards, the substrate temperature was raised again to 600 °C for further growth of 7 nm undoped GaAs. Finally, the whole layer sequence was terminated with a 145 nm thick carbon doped p-GaAs layer ( $N_{\text{A}}=1.9 \times 10^{19}$  cm<sup>-3</sup>). Finally, the sample was processed into p-i-n junction devices with small active areas ( $2 \times 2$  μm<sup>2</sup>). This, together with the controlled dot occupancy for optimized ion fluences<sup>10</sup> ensures that only single or few QDs are addressed electrically. To achieve this, thin conducting stripes of 40 μm length and 2 μm nominal width were defined in both the buried n-type and the top p-type region perpendicular to each other. For the buried n-type region, a FIB of  $\text{Be}^{2+}$  ions at a fluence of  $3 \times 10^{12}$  cm<sup>-2</sup> was used to insulate distinct regions while keeping the top (p-type) layer still conductive. The top layer was patterned by conventional photolithography and wet

<sup>a)</sup>Electronic mail: cedrik.meier@upb.de.

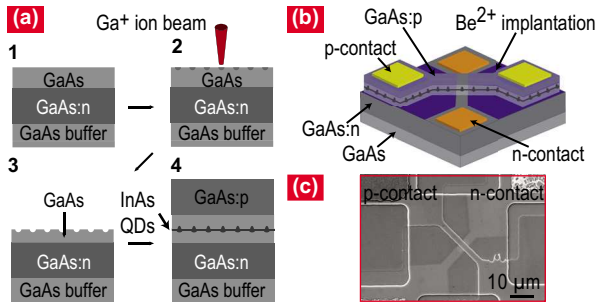


FIG. 1. (Color online) (a) Layer sequence for the p-i-n devices. (b) Schematic layout of site-selective QD light emitting  $\mu$ -diode. (c) SEM image of QD  $\mu$ -LED.

etching. In between the perpendicular oriented conducting stripes the QD layer was embedded in the intrinsic region, such that the QDs in the intersection are effectively contacted in an n-i-p structure. Ohmic contacts were fabricated using standard sequences for p- and n-contacts (Au/Zn and Au/Ni/Ge). A schematic layout of the layer structure and the device is shown in Fig. 1(a) together with an SEM image.

First, the structural morphology of the FIB patterned surfaces was studied for fluences between  $10^4$  and  $10^7$  ions/spot. Figure 2 shows at low fluences humps with an average height of 1 nm. Above  $7.7 \times 10^4$  ions/spot selective sputtering and redeposition around the center occurs, leading to small central depressions with a pronounced ring shaped structure. A further increase leads to deeper depressions and a more distinct ring structure. The AFM linescan shows that the central depression is  $\sim 1$  nm deep. For fluences of  $1.7 \times 10^6$  ions/spot, the depression depth increases up to 2 nm with a protruded ring around its edges. This is explained as follows: initially, a transition from crystalline to amorphous occurs, followed by the sputter regime with further increase in irradiated ion density. As a result, nanohumps are formed by local volume enhancement, as the density of the amorphous material is lower than that of crystalline material. The Gaussian-like beam profile explains the fact that the sputtering is first observed in the central region while in the surrounding region amorphization occurs. Redeposited material adds to the ring formation. Direct growth of InAs on these structures leads to clusters instead of QD formation.<sup>10</sup> To

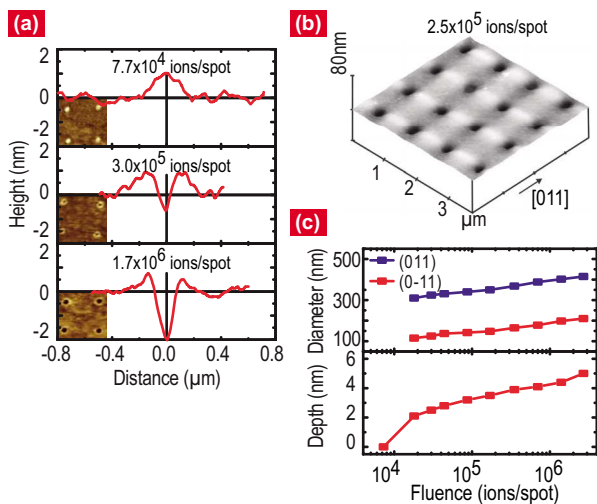


FIG. 2. (Color online) (a) Linescan topography measurements of implanted spots. Insets: Corresponding AFM images on patterned surfaces. (b) AFM measurement of annealed surface. (c) Depth and diameter of nanohumps.

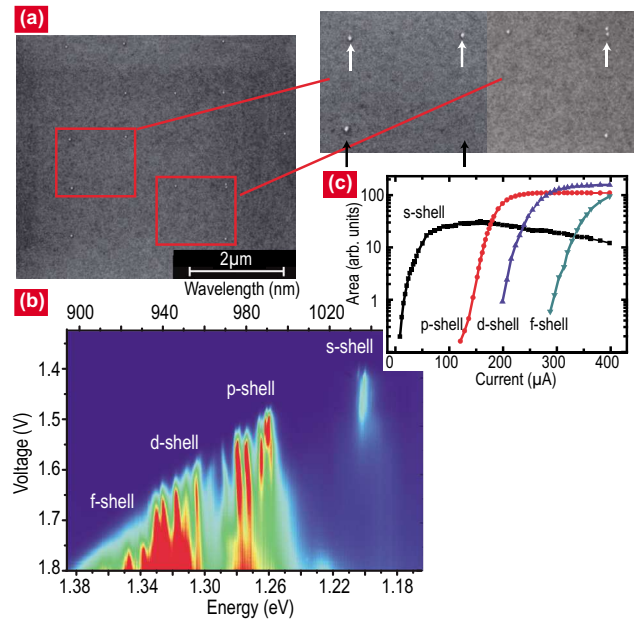


FIG. 3. (Color online) (a) SEM image of site-selectively grown InAs QD array at  $2.5 \times 10^5$  ions/spot. (b) EL spectra from a light emitting  $\mu$ -diode featuring an intentionally positioned single QD. (c) Integrated areal intensity of QD states.

remove defects and dislocation loops, *in situ* annealing is essential after FIB patterning. Therefore, we inspected the surface morphology of thermally processed surfaces. At low fluences ( $4 \times 10^4$  ions/spot), no signatures of depressions and humps are observed. At higher fluences, depressions without ring structures around the edges are observed. An AFM topography image of these shallow depressions (fluence  $\sim 2.5 \times 10^5$  ions/spot) is shown in Fig. 1(b). The depressions are more elongated along the [011] direction, with a size of  $\sim 150 \times 350$  nm<sup>2</sup>. This is caused by the thermally activated surface diffusion length of adatoms in the [011] and  $[0\bar{1}1]$  directions of the GaAs(001) surface. Due to different activation energies, at a substrate temperature of 760 °C, the surface diffusion is enhanced more along [011] direction.<sup>11</sup> The depth and lateral dimensions of the nanodepressions increase with ion fluence as shown in Fig. 2(c).

In the next step, the deposited InAs amount was fine-tuned to achieve single dot occupancy on the fabricated depressions. At or above 1.7 ML InAs, QD nucleation was observed as well on the FIB implanted spots as well as in between. Below 1.7 ML of InAs, site-selective growth in the shallow depressions occurs, without any QDs in between. The best results have been achieved for deposition of InAs between 1.53 and 1.59 MLs on spots implanted with a fluence of  $2.5 \times 10^5$  ions/spot. Figure 3(a) shows the results for these parameters. For this process, almost 52% of the sites

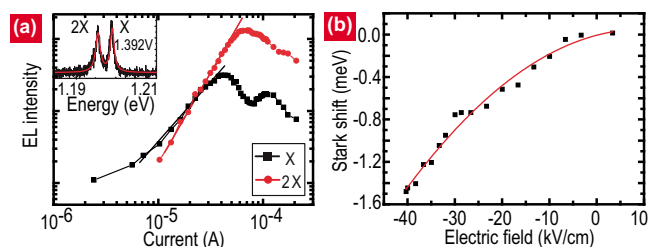


FIG. 4. (Color online) (a) Dependence of exciton (X) and biexciton (2X) lines on injection current. (b) Stark shift of the exciton (X) line.

are occupied with single QDs. However, also a nonvanishing probability for the formation of double-dot structures exists [inset of Fig. 3(a)], which could be interesting for the study of moleculelike states. The formation mechanism for the site-selective QD growth on the shallow depression is follows: The depressions have a concave curvature and are thus not as energetically favorable as the flat GaAs (001) surface. The center of the depression forms a minimum in the chemical potential, as it is surrounded by oblique high-index planes.<sup>6,8</sup> This results in a gradient, which is the driving force for the In adatom migration toward the center. This migration is only limited by the diffusion length, which can exceed 1  $\mu\text{m}$ .<sup>6</sup> Thus, the critical layer thickness is first reached in the center, where QD nucleation starts initially.

In the next step, the performance of micron sized p-i-n devices with optimized growth parameters was studied under electrical injection conditions. Using I-V measurements, the devices were characterized electrically, showing rectifying diode-like behavior with early onset voltage of  $\sim 0.5\text{V}$ , that is governed at forward bias by the contact series resistance. Figure 3(b) shows EL spectra of the device at  $T=4\text{ K}$  for different bias voltages  $V_B$  (low resolution  $\sim 0.75\text{ meV}$ ). Distinct emission lines from excitonic states are observed, arising from a single site-selectively grown QD. At low bias ( $V_B=1.380\text{ V}$ ), *s*-shell emission is observed. With increase in bias voltage, emission from the *p*-shell and higher shells is observed. The observed *s*-shell/*p*-shell energy splitting is 60 meV, comparable to other reports.<sup>12,13</sup> The dependence of the integrated areal intensity on the injection current for the different QD shells is depicted in Fig. 3(c). The successive saturation of the shells is a clear signature of shell filling effects of a single QD.<sup>4,13</sup> At high spectral resolution ( $\sim 125\text{ }\mu\text{eV}$ ) within the *s*-shell, different excitonic lines were observed. Figure 4(a) shows the EL intensity for the first two transitions. At low currents, a sharp line is observed at  $\sim 1.991\text{ eV}$ , whose intensity increases linearly with the current. We identify this line with the single uncharged exciton (X) within a single QD. At higher currents, the X line weakens and a second strong line appears at 3.5 meV lower energy. This line increases quadratically with the current and is therefore attributed to the biexciton transition (2X). The exciton–biexciton splitting is comparable to previous results.<sup>13,14</sup> The strength of the X line drops due to competition with the 2X state [Fig. 4(a)]. The linewidth of the X line at lowest bias is  $\sim 650\text{ }\mu\text{eV}$ , comparable to previous reports on site-controlled QDs (Refs. 8 and 9) but higher than purely optically pumped QDs without positioning.<sup>12</sup> As seen in the inset, the line shape is not Gaussian as reported for other single QD systems. Instead, we observe a Lorentzian profile for both X and 2X. We suggest that these linewidths are due to ultrafast ( $\Delta t \approx 500\text{ fs}$ ) phase-breaking interactions with the p- and n-doped regions. Stuffer *et al.*<sup>15</sup> demonstrated that such interactions can be reduced by increasing the distance between QD and the doped layers, resulting in linewidth down to 4  $\mu\text{eV}$ . Due to the close proximity with the highly doped contacts, the degradation of EL linewidth due to charges and defects and the FIB patterned interface cannot fully be assessed here.

Increasing forward bias also leads to a shift in peak energy of the EL lines, indicating a quantum confined Stark

effect.<sup>16</sup> Under weak injection, a blueshift up to  $\sim 1.5\text{ meV}$  of the X line is found. The forward bias reduces the effective electric field around the QD toward flat band conditions, resulting in higher emission energy [Fig. 4(b)]. The Stark shift can be described by the expression  $\Delta E_X(F) = pF + \beta F^2$ , where  $p$  is the exciton dipole moment and  $\beta$  the polarizability of the state.<sup>16</sup> From a fit to the experimental data [solid line in Fig. 4(b)] we obtain  $p = 2 \times 10^{-29}\text{ cm}$  (equivalent to an electron-hole separation of 0.13 nm) and a  $\beta = -57e\text{ nm}^2/\text{V}$ . These values are in good agreement with previously results<sup>16,17</sup> and indicate the good morphological quality, which leads to an excellent electronic structure of the QDs. The polarity of the dipole moment indicates that the electron component of the wave function is located below the hole in the dot at  $F=0$ , signifying In enrichment toward the QD apex.<sup>16</sup>

We have demonstrated a concept for fabrication of site-selective QDs and their integration into a fully electrically controllable structure. The spectroscopic results show that the single dot character is preserved and individual excitonic states can be studied. The observed exciton linewidth is limited by Coulomb interactions with the doped regions and does not impose a principal limit. We believe that this method has strong potential for future quantum devices.

Funding by BMBF via NanoFutur & nanoQUIT programs (03X5509, 01BM466 and 01BM451).

<sup>1</sup>D. Bimberg, M. Grundmann, and N. N. Ledentsov, *Quantum Dot Heterostructures* (Wiley, New York, 1999).

<sup>2</sup>P. Michler, *Single Semiconductor Quantum Dot* (Springer, Berlin, 2003).

<sup>3</sup>Z. Yuan, B. E. Kardynal, R. M. Stevenson, A. J. Shields, C. J. Lobo, K. Copper, N. S. Beattie, D. A. Ritchie, and M. Pepper, *Science* **295**, 102 (2002).

<sup>4</sup>R. Schmidt, U. Scholz, M. Vitzethum, R. Fix, C. Metzner, P. Kailuweit, D. Reuter, A. D. Wieck, M. C. Hübner, S. Stuffer, A. Zrenner, S. Malzer, and G. H. Döhler, *Appl. Phys. Lett.* **88**, 121115 (2006).

<sup>5</sup>C. L. Salter, R. M. Stevenson, I. Farrer, C. A. Nicoll, D. A. Ritchie, and A. J. Shields, *Nature (London)* **465**, 594 (2010).

<sup>6</sup>B. D. Gerardot, G. Subramanian, S. Minvielle, H. Lee, J. A. Johnson, W. V. Schoenfeld, D. Pine, J. S. Speck, and P. M. Petroff, *J. Cryst. Growth* **236**, 647 (2002).

<sup>7</sup>P. Alonso-González, L. Gonzalez, Y. Gonzalez, D. Fuster, I. F. Martinez, J. M. Sanchez, and L. Abelmann, *Nanotechnology* **18**, 355302 (2007).

<sup>8</sup>P. Atkinson, O. G. Schmidt, S. P. Bremner, and D. A. Ritchie, *C. R. Phys.* **9**, 788 (2008).

<sup>9</sup>S. Kiravittaya, A. Rastelli, and O. G. Schmidt, *Rep. Prog. Phys.* **72**, 046502 (2009).

<sup>10</sup>M. Mehta, D. Reuter, A. Melnikov, A. D. Wieck, and A. Remhof, *Appl. Phys. Lett.* **91**, 123108 (2007).

<sup>11</sup>M. Hata, T. Isu, A. Watanabe, and Y. Katayama, *J. Vac. Sci. Technol. B* **8**, 692 (1990).

<sup>12</sup>B. D. Gerardot, D. Brunner, P. A. Dalgarno, P. Öhberg, S. Seidl, M. Kroner, K. Karrai, N. G. Stoltz, P. M. Petroff, and R. J. Warburton, *Nature (London)* **451**, 441 (2008).

<sup>13</sup>S. Raymond, X. Guo, J. L. Merz, and S. Fafard, *Phys. Rev. B* **59**, 7624 (1999).

<sup>14</sup>S. Rodt, R. Seguin, A. Schliwa, F. Guffarth, K. Pötschke, U. W. Pohl, and D. Bimberg, *J. Lumin.* **122–123**, 735 (2007).

<sup>15</sup>S. Stuffer, P. Ester, A. Zrenner, and M. Bichler, *Appl. Phys. Lett.* **85**, 4202 (2004).

<sup>16</sup>P. W. Fry, I. E. Itskevich, D. J. Mowbray, M. S. Skolnick, J. J. Finley, J. A. Barker, E. P. O'Reilly, L. R. Wilson, I. A. Larkin, P. A. Maksym, M. Hopkinson, M. Al-Khafaji, J. P. R. David, A. G. Cullis, G. Hill, and J. C. Clark, *Phys. Rev. Lett.* **84**, 733 (2000).

<sup>17</sup>J. J. Finley, M. Sabathil, P. Vogl, G. Abstreiter, R. Oulton, A. I. Tartakovskii, D. J. Mowbray, M. S. Skolnick, S. L. Liew, A. G. Cullis, and M. Hopkinson, *Phys. Rev. B* **70**, 201308 (2004).